MARITIME TRANSPORTATION RESEARCH AND EDUCATION CENTER
TIER 1 UNIVERSITY TRANSPORTATION CENTER
U.S. DEPARTMENT OF TRANSPORTATION

Port Infrastructure Resilience Through Combined Wind-Surge Demand Characterization

July 1, 2020 to August 30, 2023

Prepared by:

Kaley Callaway
Gary S. Prinz, PhD, PE (Project PI)

Department of Civil Engineering,
University of Arkansas, Fayetteville,
4190 Bell Engineering Center,
Fayetteville AR, 72701

August, 2023

FINAL RESEARCH REPORT
Prepared for:
Maritime Transportation Research and Education Center

University of Arkansas
4190 Bell Engineering Center
Fayetteville, AR 72701
479-575-6021

ACKNOWLEDGEMENT

This material is based upon work supported by the U.S. Department of Transportation under Grant Award Number 69A3551747130. The work was conducted through the Maritime Transportation Research and Education Center at the University of Arkansas.

DISCLAIMER

The contents of this report reflect the views of the authors, who are responsible for the facts and the accuracy of the information presented herein. This document is disseminated in the interest of information exchange. The report is funded, partially or entirely, by a grant from the U.S. Department of Transportation's University Transportation Centers Program. However, the U.S. Government assumes no liability for the contents or use thereof.

Executive Summary

The United States economy is reliant on maritime transportation for 70% of imports and exports. Structures that are integral to the operation of ports, such as cranes, are jeopardized when tropical storms approach land. While wind is the only environmental load used to design dockside container cranes, storm surge often accompanies severe wind events and can create large structural loads. This study focuses on determining coupled storm-surge demands and the effect of waves on dockside container cranes. A damage index prediction tool that considers both maximum wind speed and storm surge height is developed and applied to historical hurricane data for effectiveness. Comparisons of the new damage index with traditional damage indices based solely on wind-speed indicate that the coupled wind-surge model more accurately represented the damage of the selected hurricanes. Analytical models in a parametric study investigate the influence of combined wind and water forces on port-type structures and an experimental model is created to validate the analytical results. Results from the parametric investigations indicate that when surge conditions are considered, wave height and wave type have more impact on the structural demands than wind speed. For loading scenarios impacted by surge, there was no identifiable increase in stress on the structure when wind speed increased. The developed wind-surge damage index and analytical model findings suggest that both storm surge and wave loading should be considered in port infrastructure design to reduce damage costs and improve resiliency.

Table of Contents

List of Figures

List of Tables

1. Introduction

Coastal ports in the United States are integral to the economy; 70% of imports and exports are facilitated through maritime transportation [1]. The ports of Los Angeles and Long Beach handle over $250 billion of transported goods annually and directly or indirectly provide over 600,000 jobs to the economy [2]. Coastal ports are at risk of experiencing high winds and storm surges that cause millions of dollars in infrastructure damage due to their proximity to the ocean. Hurricane Katrina caused Alabama's Port of Mobile at least $30 million in damages, and mostly due to storm surge [3]. A delay of operation caused by damage to port infrastructure imposes delays in operation, leading to economic ramifications in the immediate area and further down the supply chain. Coastal ports cannot ship mass loads of products by sea without dockside container cranes to load and unload the shipping containers. A lack of dockside cranes can lead to weeks of delay in the transport of goods. After Hurricane Laura in 2020, the Port of Lake Charles had no functioning loading or unloading cranes out of the four total at the port. Lake Charles produces 6% of the nation's gasoline, so multiple areas around the country were affected by the port being unserviceable [4, 5].

Current approaches for estimating structural demands from wind and storm surge do not adequately compare the effects of combined wind and water loads. Some studies combine wind-wave demands, or investigate wind or wave demands separately. In [6], the combined wind-wave study attempted to estimate hurricane destruction potential by considering integrated kinetic energy. Integrated kinetic energy is the kinetic energy per unit volume of the storm domain volume containing sustained surface wind speeds within a certain range. Kinetic energy relates to wind destructive potential because it scales with wind pressure on a structure. It is relevant to storm surge because wind speeds affect the size of waves and elevated water levels at the shore. [6] was

limited to historical data used to retroactively assess the damage potential of storms. In [7], researchers aimed to understand combined wind-surge demands using smartphone data and geotagged photographs to accumulate structural details and damage observations. It was limited to only one hurricane event, Hurricane Harvey. Preliminary observations showed potential wind-surge combined loading effects. Research in [8] investigated only hurricane wind damage to cranes located on docks. Cranes are designed based on historical wind speed data; this paper investigates recent trends in hurricane wind loads to determine if crane design standards should be updated. The study in [8] indicated that hurricane wind speeds in 2009 had not increased much relative to previous events; however, the size and duration of storms had increased. Tsunami loads on structures were considered in [9], using photographic observations of the damage done by the various forces of past tsunamis. Note that there were no analytical or experimental models performed in [9], but rather provides a data index of damage caused by the Tohoku Tsunami and lessons learned from the damage.

This research aims to improve the understanding of wind and surge-wave demands on port infrastructure and to develop hazard demand models to aid improvements to infrastructure design. Analytical and experimental efforts considering simultaneous wind-surge and wave impacts were developed, and historical data was collected to improve damage prediction of wind-surge events. Because dockside container cranes are integral to the operation of coastal ports, structures of this type were considered for the combined wind-surge and wave investigations.

2. Storm Severity Prediction Tool Based on Historic Data from Port Storm Surge Events

When a tropical storm is approaching, it is helpful to have a system for predicting the severity of the storm so that preparations can be made before it makes landfall. Every tropical storm has different characteristics with varying levels of severity; therefore, each storm causes

varying levels of damage to infrastructure. The Saffir-Simpson (SS) scale is commonly used by the National Hurricane Center [10] to quantify storm severity; however, this scale only uses one metric, maximum sustained wind speed for 1 minute, to determine the severity of potential infrastructure damage. The SS method puts tropical storm events into 1 of 5 categories based on the maximum wind speed. Category 1 storm events have low (74-95 mph) wind speeds while Category 5 events have extremely high (157+ mph) wind speeds.

Wind speed alone may not be an accurate representation of the potential for damage caused by a storm event. For example, Hurricane Katrina was a Category 3 hurricane when it made landfall, but it is the second costliest hurricane to date with a total of $118.89 billion (2021 USD) in damages [11]. In comparison, Hurricane Michael was also a Category 5 hurricane that amounted to only $28.48 billion (2021 USD) [12]. Additional metrics are needed for storm damage prediction and severity calculation of storms.

In addition to severe winds, coupled storm surge demands contribute to infrastructure damage and loss. The SS scale mentioned does not consider storm surge due to the inconsistency between maximum sustained wind speed and maximum level of storm surge [13]. To highlight the potential for differing surge heights (with differing hurricane categories), Hurricane Katrina, a Category 3 based on wind speed, had a 28 ft storm surge, while Hurricane Michael, a Category 5 based on wind speed, had only 7.5 ft of storm surge. Hurricane Ike, a Category 2 based on wind speed, had 20 ft of storm surge [14].

Other researchers at StormGeo, a weather intelligence company, expanded on the wind characteristics that need to be considered when they created the Hurricane Severity Index (HSI) [15]. The HSI considers the total area of the tropical storm that produced wind in addition to maximum sustained wind speed, V_{max} . To label a tropical storm using this method, severity points

are assigned to each component and added together. Severity points for the maximum sustained wind speed, W, are calculated using Equation 1. Note the HSI did not consider tropical storms with maximum sustained wind speeds below 30 mph, and the maximum points allotted for W are 25.

$$W = \left(\frac{V_{max}}{30}\right)^2 \qquad \text{Equation 1}$$

The area of the tropical storm that produces a particular wind speed is called the wind field. The wind field helps determine the time period a particular wind speed will hit one geographical location. A larger wind field indicates one location will experience a wind speed for a longer time period. Hurricanes are often asymmetrical, so StormGeo determined an effective wind field radius for each storm for better comparison. The effective wind field radius estimates the area of a hurricane with a certain wind speed (see Figure 1). A tropical storm has various wind speeds throughout, so one tropical storm requires multiple wind fields to be considered.

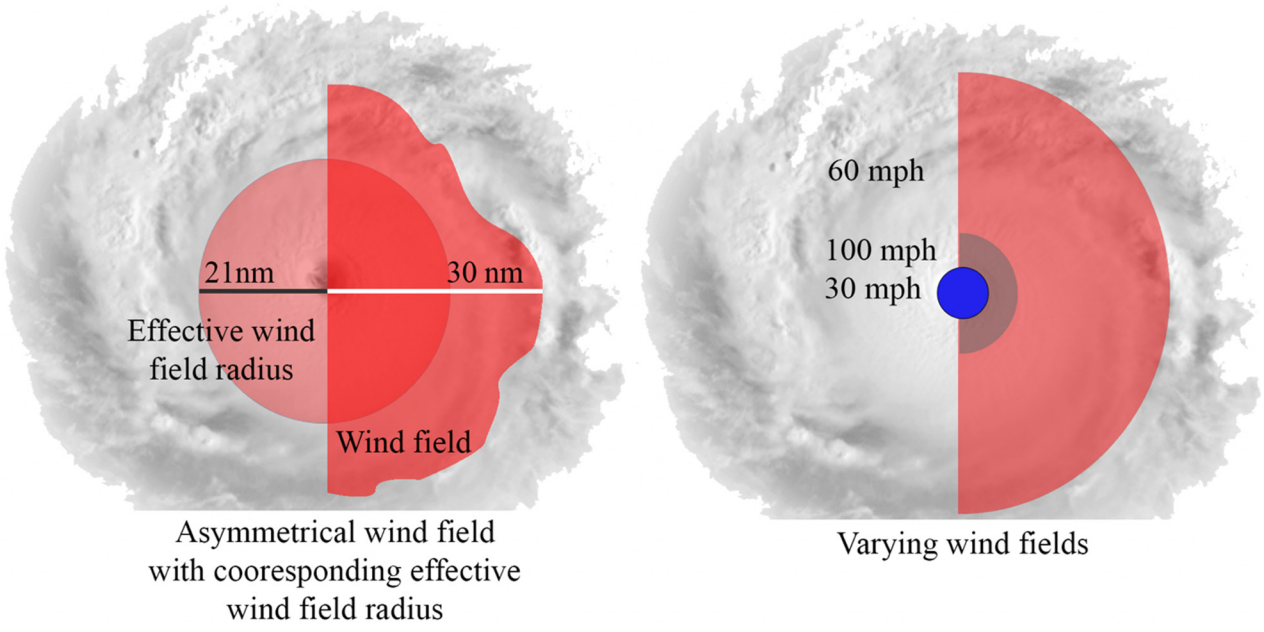

Figure 1. Visual of a wind field and why the effective radius is needed.

Points are assigned for each wind field size and wind speed combination, and point values are added together for a composite wind field score. For example, Figure 2 details point value assignments based on effective wind field radius and the wind intensity in that wind field. Figure 2 illustrates a wind field with a 40mph wind speed and an effective wind field radius of 90 nautical miles (nm); considering the HIS, 3 points would be assigned to that wind field. In the HIS, the wind field and intensity points are added together for a composite score. When wind field scores reach 25, the maximum score is achieved. The HSI considers both wind field and maximum sustained wind speed, but neglects a rise in sea level that occurs when a tropical storm approaches land.

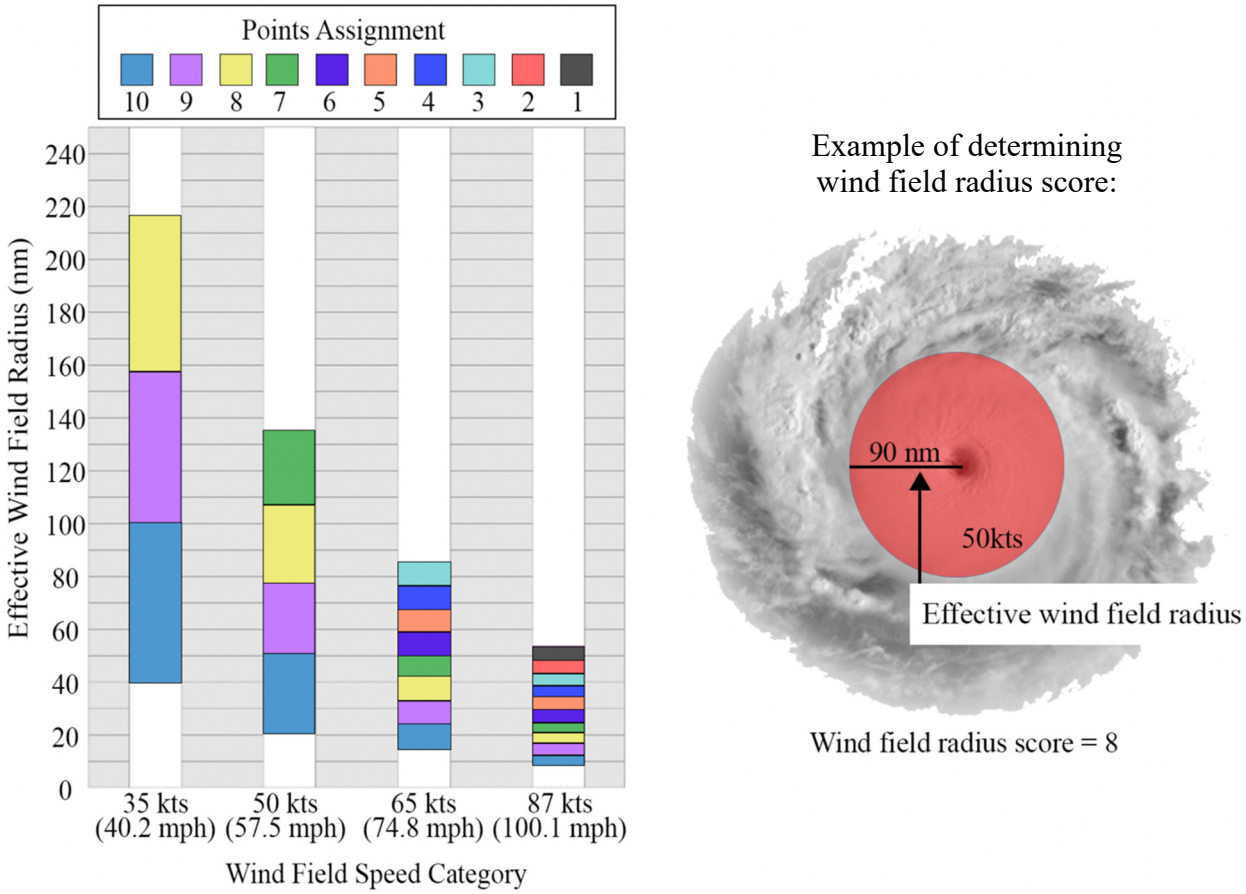

Figure 2. HSI wind field point assignments. Chart obtained from [15].

In this study, a modified storm damage index (named the Wind-Surge Index, WSI) is developed based on the SS and HSI, to account for damaging effects related to coupled wind and storm surge demands. To develop a damage index incorporating storm surge effects, storms are not placed in a category based on maximum sustained wind speed but rather points are assigned to each individual wind and surge parameter chosen to characterize the strength of the tropical storm (similar to a modified HSI). In this new damage index, points for storm surge are determined by the height of surge as will be discussed in following paragraphs.

The WSI method developed herein, modifies the HSI score with added effects/points from a surge score. The maximum possible score of a tropical storm event in the WSI is 50 points, similar to the HSI method. The wind and storm surge each comprise half of the scoring, so the HSI score is divided by two and added to the storm surge score. The minimum requirement for classification as a hurricane based on the National Hurricane Center is sustained winds of 74-95 mph [10]. Storms with these wind speeds can be expected to cause 4-5 ft of storm surge [16], so this study did not consider any surge 3 ft or below. To calculate the points assigned, 3 ft was subtracted from the maximum surge. For example, Hurricane Katrina produced 30 ft of surge. The points assigned to Hurricane Katrina are 27 = 30 – 3. This creates a linear relationship between the surge height and points assigned and was based on the relationship between water depth and pressure exerted on an object. The WSI for coupled wind-surge damage prediction is calculated as follows:

Step 1: Divide HSI rating by 2 (maximum score = 25) for wind speed score.

Step 2: Determine surge height (ft) and subtract 3 (maximum score = 25) for surge score.

Step 3: Add wind and surge scores together for a composite out of 50.

To determine how well this scoring method predicts the severity of a storm, economic losses from historical storm events will be evaluated with the WSI and compared to the traditional SS and HSI approaches. For direct comparison, economic losses of past tropical storm events are normalized to one year for comparison [17, 18]. Events from the years 2004 to 2020 are considered. The dollar values were converted from the year of impact, y, to 2021. Multiple changing societal conditions needed to be considered when converting, and the first was population. An area with a low population will likely have less infrastructure to damage than that of a highly-populated area. Though each hurricane that makes landfall typically affects more than one county due to tornadoes, rainfall, wind, etc., this study only considered the county most impacted by risen surge levels. These counties were on the coast and more likely to contain the port infrastructure in question.

The county population factor, P_y, is a ratio of the county population, CP, in 2021 to the year of hurricane landfall [19]. The United States Census Bureau publishes county population total estimates every year. The United States census is only taken every 10 years, so every year that is not a multiple of 10 is an estimate [20]. Estimates for 2021 have not been released, so the population was projected using 2010 and 2020 census data. Values for populations in relevant years is provided in Table 1. This is an example of how P_y was determined: 2005 Hurricane Katrina landed in New Orleans, LA of Orleans Parish. In 2005, the population of Orleans Parish is interpolated to be 414252. The 2021 population is extrapolated to be 388014. P_y = 0.94 = 388014/414252.

Table 1. County population data.

County	State	2004	2005	2008	2010*	2011	2012	2016	2017	2018	2019	2020*	2021
Mobile	AL	397959			412992							414809	414991
Bay	FL				168852					186240		175216	175852
Collier	FL		307452		321520							375752	381175
Escambia	FL		298339		297619							321905	324334
Lee	FL	522431			618754							760822	775029
Miami-Dade	FL				2496435							2701767	2722300
St. Lucie	FL	228548			277789							329226	334370
Monroe	FL				73090				76483			82874	83852
Calcasieu Parish	LA				192768							216785	219187
Lafayette Parish	LA				221578						244390	241753	243771
Orleans Parish	LA		494294		343829		369787					383997	388014
Cameron Parish	LA		9846		6839							5617	5495
Terrebonne Parish	LA			111453	5252							109580	120013
Atlantic	NJ				274549		274629					274534	274533
Brunswick	NC				107431							136693	139619
Carteret	NC				66469	67418						67686	67808
New Hanover	NC				202667					232256		225702	228006
Charleston	SC				350209			396880				408235	414038
Harris	TX			3938580	4092459							4731145	4795014
Nueces	TX				340223				361235			353178	354474

*Census data, not a population estimate

Inflation, the general increase in prices and decrease in purchasing power of money, is represented by the implicit price deflator for gross domestic product (GDP deflator) [19]. Gross domestic product is the total monetary value of final goods and services in the United States. A final good or service is one bought by the final user. The GDP deflator measures the changes in the price of all final goods and services. Every quarter there is a GDP deflator value released by the U.S. Bureau of Economic Analysis [21]. To calculate the GDP deflator of a calendar year an average of the quarter values in the same year was taken. Because the final quarter of 2021 was not released, an average of the available three quarters for 2021 was used. The inflation factor, I_y, is a ratio of the 2021 GDP deflator to the GDP deflator of the year the hurricane made landfall. Following the Hurricane Katrina example, the GDP deflator is 87.5 and 117.39 for 2005 and 2021 respectively. I_y = 1.342 = 117.39/87.5. For a list of all GDP values refer to Table 2.

Over time people accumulate more wealth by owning more items than the average person did in previous years. Some items people own increase in value over time. To capture the change in wealth, wealth per capita is also an adjustment factor for the normalization of monetary hurricane damage [19]. National wealth represented wealth per capita, but inflation and population affect national wealth. Adjustment factors are needed to consider national wealth without influence of inflation and population. National wealth is represented by the current-cost net stock of fixed assets and consumer durable goods, or fixed assets [22]. The population of the country is used because wealth per capita is estimated for the entire United States. Similar to the county populations, years in-between the census are estimated by the US Census Bureau. Fixed asset data for 2021 has not been released, so the wealth per capita factor is normalized to 2020. The population and inflation adjustments for wealth per capita are also to 2020. The fixed assets ratio, $V_{2020/y}$, is the ratio of fixed assets in year 2020 to year y, the year of hurricane landfall. Following

the 2005 Hurricane Katrina example, $V_{2020/y} = 1.7 = \frac{73{,}947.4}{43{,}399.2}$. The inflation adjustment, $I_{2020/y}$, for Hurricane Katrina (compared to year 2020, not 2021 as it was for the general inflation factor) is $1.3 = \frac{113.6}{87.5}$. The national population adjustment, $NP_{2020/y}$, is the ratio of the national population in year 2020 to year y. $NP_{2020/y} = 1.1 = \frac{331{,}449{,}281.0}{294{,}083{,}722.0}$. Therefore, the adjusted wealth per capita factor, W_y, is $1.2 = 1.7/1.3/1.1$ as calculated using Equation 2. For a list of all fixed assets and national population data, refer to Table 3 which summarizes data used to calculate the wealth per capita factor used to normalize the hurricane event costs to 2021. For the wealth per capita factor only, the values were normalized to 2020 due to a fixed asset value not yet available for 2021. The years 2010 and 2020 are census years, meaning the US population value is not an estimate. Every year aside from 2010 and 2020 are estimated values provided by [20].

All inflation, county population, and wealth per capita values considered an be found in Table 4. Note that in Table 4, all factors are calculated to normalize the hurricane events costs to the year 2021. The year listed represents the year those numbers were normalized. The national population and 2020 GDP ratio values were used in the wealth per capita factor. The county population and 2021 GDP ratios were used for their respective factors. Following is a list of each event with its reference(s) for surge height, location, wind speed, and cost: Barry [27], Hanna [28], Delta [29], Zeta [30], Isaac [31, 32], Dennis [33], Isaias [34], Gustav [35], Rita [36], Sally [37], Matthew [38], Irene [39], Frances [40], Laura [4, 41], Michael [12], Charley [42], Florence [43], Ivan [44], Wilma [45], Ike [14], Irma [46], Sandy [47], Katrina [11], Harvey [48].

$$W_y = \left(V_{2020/y}\right)/\left(I_{2020/y}\right)/\left(NP_{2020/y}\right) \qquad \text{Equation 2}$$

Table 2. GDP deflator values for calculating inflation.

Date	GDP Deflator	Date	GDP Deflator
1/1/04	83.895	1/1/13	101.141
4/1/04	84.569	4/1/13	101.428
7/1/04	85.112	7/1/13	101.906
10/1/04	85.770	10/1/13	102.515
1/1/05	86.453	1/1/14	102.942
4/1/05	87.082	4/1/14	103.525
7/1/05	87.874	7/1/14	103.977
10/1/05	88.585	10/1/14	104.15
1/1/06	89.209	1/1/15	104.113
4/1/06	90.000	4/1/15	104.677
7/1/06	90.628	7/1/15	104.989
10/1/06	90.967	10/1/15	104.979
1/1/07	91.839	1/1/16	104.895
4/1/07	92.453	4/1/16	105.636
7/1/07	92.933	7/1/16	105.929
10/1/07	93.327	10/1/16	106.487
1/1/08	93.655	1/1/17	107.025
4/1/08	94.130	4/1/17	107.369
7/1/08	94.840	7/1/17	107.903
10/1/08	95.065	10/1/17	108.67
1/1/09	95.018	1/1/18	109.261
4/1/09	94.852	4/1/18	110.234
7/1/09	94.954	7/1/18	110.597
10/1/09	95.267	10/1/18	111.175
1/1/10	95.526	1/1/19	111.514
4/1/10	95.992	4/1/19	112.152
7/1/10	96.282	7/1/19	112.517
10/1/10	96.846	10/1/19	112.978
1/1/11	97.346	1/1/20	113.346
4/1/11	97.989	4/1/20	112.859
7/1/11	98.595	7/1/20	113.888
10/1/11	98.714	10/1/20	114.439
1/1/12	99.313	1/1/21	115.652
4/1/12	99.713	4/1/21	117.413
7/1/12	100.230	7/1/21	119.095
10/1/12	100.738		

Table 3. Data for calculating wealth per capita.

Year	US Population Estimate	Fixed Assets
2004	292108553	39609.3
2005	294784353	43399.2
2006	297649663	46808.1
2007	300511531	48889.9
2008	303381938	50486.1
2009	306112520	49645.8
2010*	308745538	50520.1
2011	311556874	52221.2
2012	313830990	53819.6
2013	315993715	56290.3
2014	318301008	58444.4
2015	320635163	59886.2
2016	322941311	62321.3
2017	324985539	64821
2018	326687501	68203.2
2019	328239523	70880.9
2020*	331449281	73947.4

*Census data, not a population estimate

Table 4. Factors calculated for normalizing the cost of historic hurricanes.

Event	Population		GDP Ratio		Weath per Capita	Event Cost in Billions	
	2021	2020	2020	2021	2020	Year y	2021
	County Population	National Population					
Barry	1.02	0.99	1.01	1.38	1.02	0.60	0.86
Hanna	1.00	1.00	1.00	1.24	1.00	1.00	1.50
Delta	1.01	1.00	1.00	1.34	1.00	3.00	3.93
Zeta	1.00	1.00	1.30	1.09	1.17	4.00	5.59
Isaac	1.10	0.95	1.00	1.11	1.00	2.00	3.43
Dennis	1.10	0.89	1.14	1.03	1.14	3.00	5.16
Isaias	1.00	1.00	1.00	1.09	1.00	5.00	5.14
Gustav	0.98	0.92	1.00	1.24	1.00	6.00	7.32
Rita	0.54	0.89	1.30	1.34	1.17	11.00	8.91
Sally	1.01	1.00	1.20	1.34	1.11	7.00	10.99
Matthew	1.08	0.97	1.34	1.38	1.23	10.00	18.28
Irene	1.02	0.94	1.00	1.03	1.00	16.00	16.62
Frances	1.47	0.88	1.07	1.03	1.08	10.00	19.67
Laura	1.01	1.00	1.34	1.17	1.23	19.00	27.70
Michael	1.01	0.99	1.20	1.06	1.11	25.00	30.56
Charley	1.51	0.88	1.16	1.05	1.15	16.00	29.66
Florence	1.03	0.99	1.03	1.38	1.04	24.00	35.53
Ivan	1.02	0.88	1.34	1.03	1.23	19.00	33.80
Wilma	1.33	0.89	1.30	1.03	1.17	20.00	32.08
Ike	1.21	0.92	1.05	1.34	1.06	38.00	65.57
Irma	1.11	0.98	1.03	1.06	1.04	50.00	61.27
Sandy	1.00	0.95	1.14	1.20	1.14	50.00	95.83
Katrina	0.94	0.89	1.30	1.17	1.17	108.00	103.92
Harvey	1.01	0.98	1.05	1.03	1.06	125.00	138.98

3. Fluid-Structure Interaction Analyses

To investigate fluid-structure interaction effects on port infrastructure, two advanced finite element models were created. The first considers a simple crane shape, a rectangular prism, to provide validation of modeling techniques against experimental measurements. In the models, an applicator is used to displace the water to simulate a wave, and the water is contained within a rectangular domain, seen in Figure 3. The second model has a detailed shape to simulate the effects of the coupled wind-storm surge forces on a dockside container crane. The dimensions of Crane 2, the detailed crane in Figure 4, are similar to a Terex dockside container crane drawing provided by Paul Bridges & Associates.

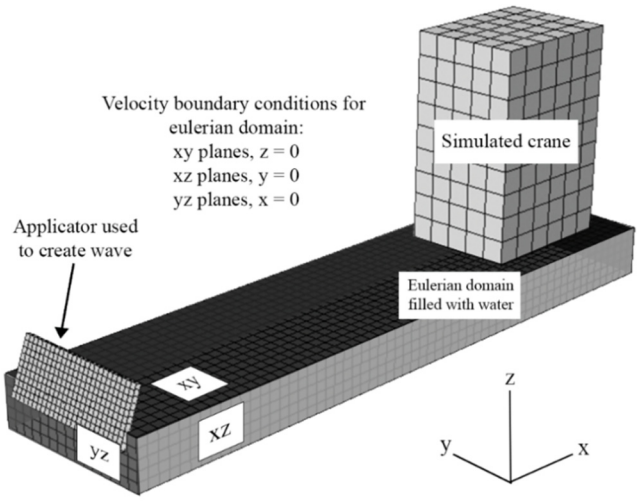

Figure 3. Boundary conditions for eulerian domain.

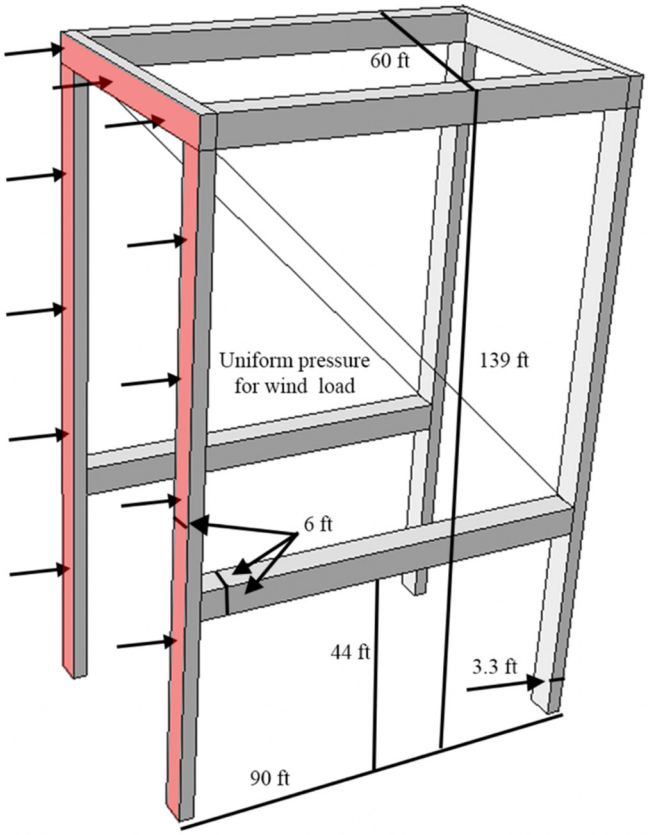

Figure 4. Crane 2, detailed crane dimensions and wind loading.

To simulate the water, a eulerian approach is used. A large rectangular domain is created from a eulerian part. A eulerian part is initially empty of material. Material must be assigned to

the part, or a section of the part, in a material pre-defined field. The commercial finite element program ABAQUS is used for each simulation to calculate the material volume fraction for each element . The percentage of an element that is filled with the material when the material is assigned. If an element is full of material, the volume fraction is one. This is done as the material flows through the mesh during the simulation. For partially full elements, the exact shape of the material within the element is not known. Abaqus interpolates between the material volume fraction of adjacent elements to estimate the shape of the material within the unknown element [23, 24]. Any space in the element that is not filled with the material is void. When viewing the animation of the model the voids in the material can be seen. To create the barriers of the domain to hold the water, velocity boundary conditions are applied. The direction perpendicular to the face of the domain has a velocity = 0.

The waves are created using an applicator to push the water and a gravity load. The applicator is a discrete rigid part that required a reference point to attach the part to some point in space. An amplitude is applied to the applicator to create motion. To tell Abaqus how quickly move the applicator, an amplitude is attached to the reference point created. A tabular amplitude is arbitrarily used. The displacement of the applicator is determined by the boundary conditions applied. A displacement/rotation boundary condition is applied to the reference point on the applicator, and the tabular amplitude is applied to that boundary condition. The applicator is moved in a diagonal (+U1, -U2) direction to displace the water. Figure 5 is provided below to illustrate the applicator movement resulting from the boundary condition.

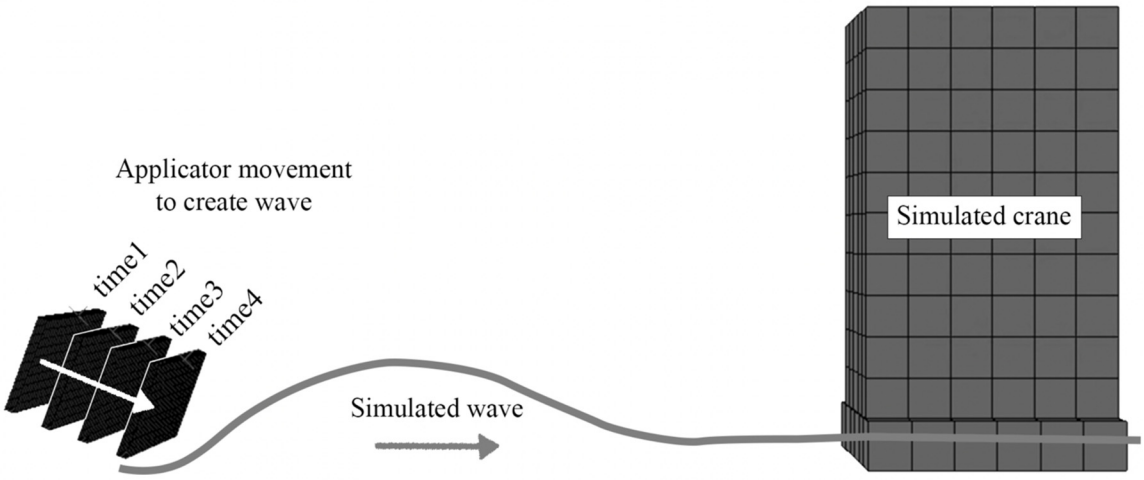

Figure 5. Progression of applicator during animation.

Pressure is applied to the yz plane of the crane to simulate the wind. The wind pressure is calculated using $0.00256(V^2)$, where the result was psf and V is mph. For a wind speed of 120mph, the equivalent wind pressure is 36.86psf.

The applicator is a discrete rigid part and the crane was a deformable shell. To allow all the parts to interact with each other, a general contact (explicit) was created for Step-1. The included surface pairs in the Contact Domain settings of the interaction are set to "All* with self". This allows all exterior features to interact (including self-contact). The interaction properties for general contact included tangential behavior with a penalty friction formulation and friction coefficient of 0.1. Normal behavior is also included with hard contact for the pressure-overclosure and allows separation after contact.

Figure 6 shows an example of the wave progression with Crane 1, along with resulting contact pressure contours. Figure 7 provides an example of the wave progression and typical contact pressures for Crane 2. In this study, simulations are performed by varying wind and surge-wave loads, including only wind and only surge-wave loading. A list of load combinations considered is included below in Table 5.

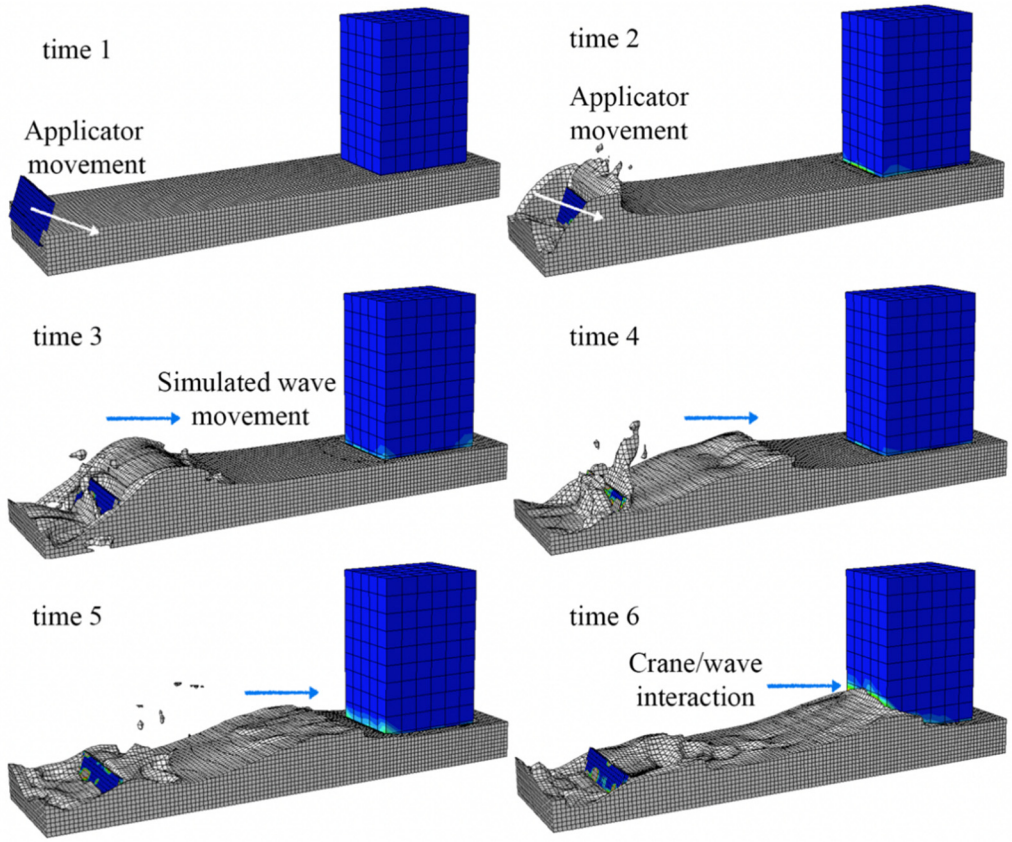

Figure 6. Progression of Crane 1 with contact pressure contours.

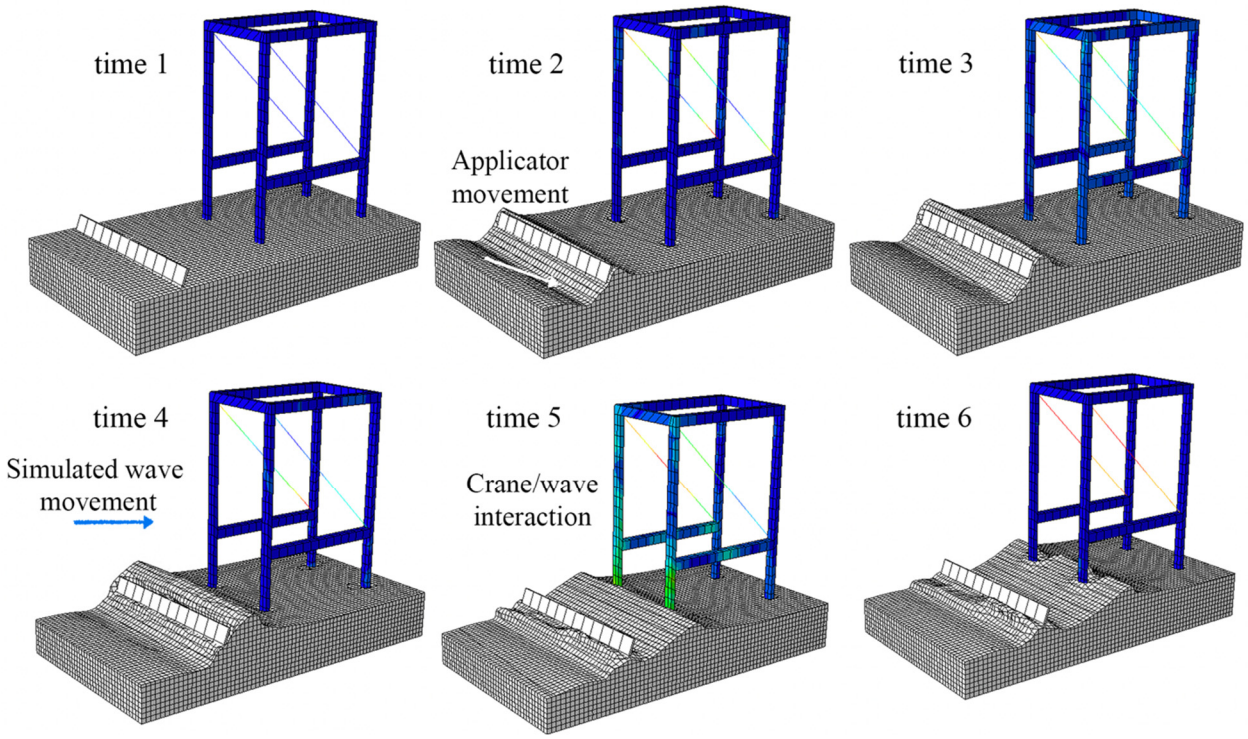

Figure 7. Progression of wave for Crane 2.

Table 5. Load combination and results for each simulation with 0ft surge.

Simulation #	Wind, mph	Wave Height, ft	Maximum Average Stress, ksf
1		40	206
2		30	290
3	120	24	210
4		20	96
5		0	1
6		40	197
7		30	205
8	100	24	181
9		20	111
10		0	2
11		40	204
12		30	226
13	80	24	199
14		20	99
15		0	1
16		40	201
17		30	188
18	60	24	199
19		20	101
20		0	1
21		40	300
22	0	30	196
23		24	190
24		20	115

4.Results and Discussion

4a. Tropical Storm Severity Prediction Tool Based on Historic Data

Figure 8, Figure 9, and Figure 10 show how the destructive rating gets more accurate when another characteristic of a storm is considered. The first 8 hurricanes listed cost less than $20 billion, but the SS rating jumps between 1 and 4 multiple times. The SS ratings showed no consistency in estimating the damage cost of a hurricane. Accounting for only maximum sustained wind speed over 1 minute does not capture how destructive a hurricane will be. The HSI rating had an improvement by including the wind field because more damage will occur to a structure being hit by 60mph winds over 30 minutes in comparison to 1 min. The Wind-Surge rating showed more consistency. The cost of hurricanes and ratings had a general rising trend. It also provided

some distinction between hurricanes. For example, Michael, Wilma, Ivan, and Katrina all have a similar HSI rating, but when surge is considered, Katrina rises significantly and there is a distinction between the other three.

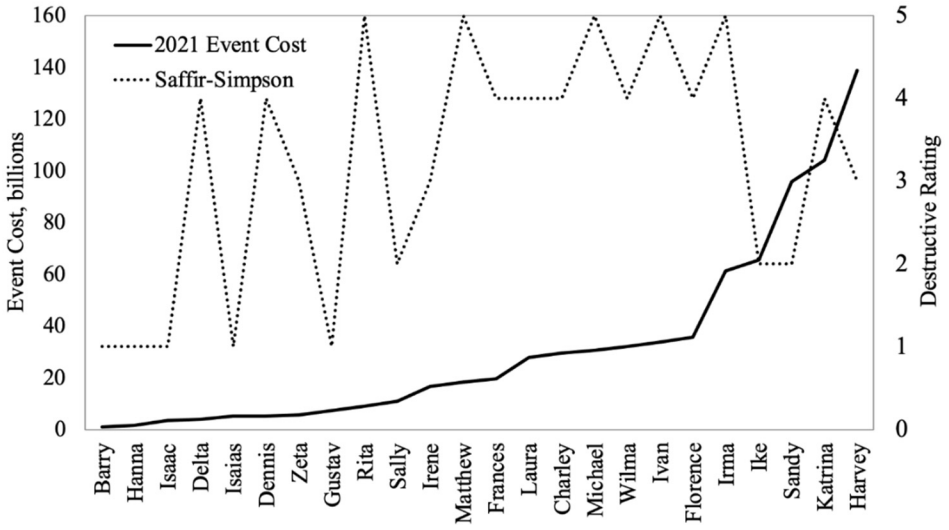

Figure 8. Saffir-Simpson vs. 2021 event cost.

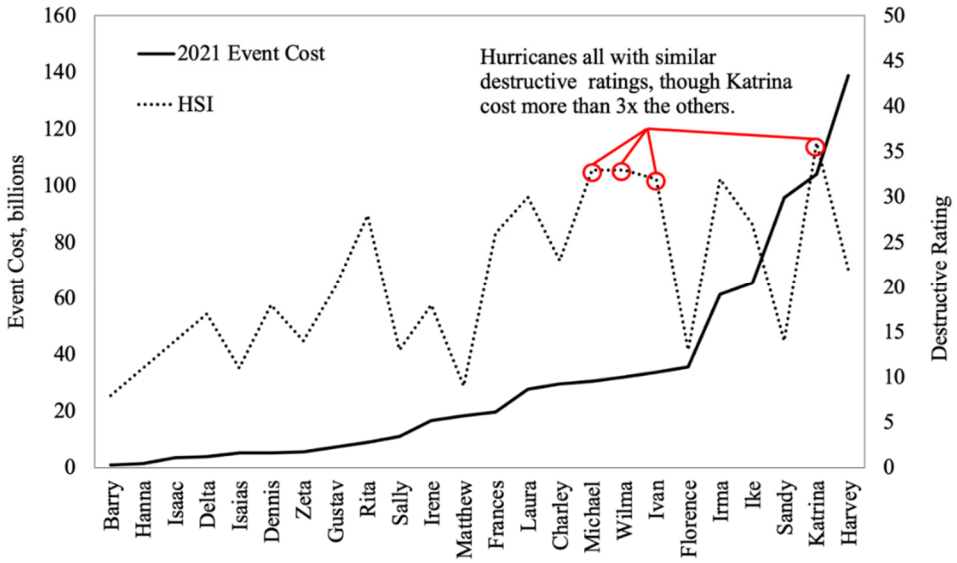

Figure 9. HSI vs. 2021 event cost.

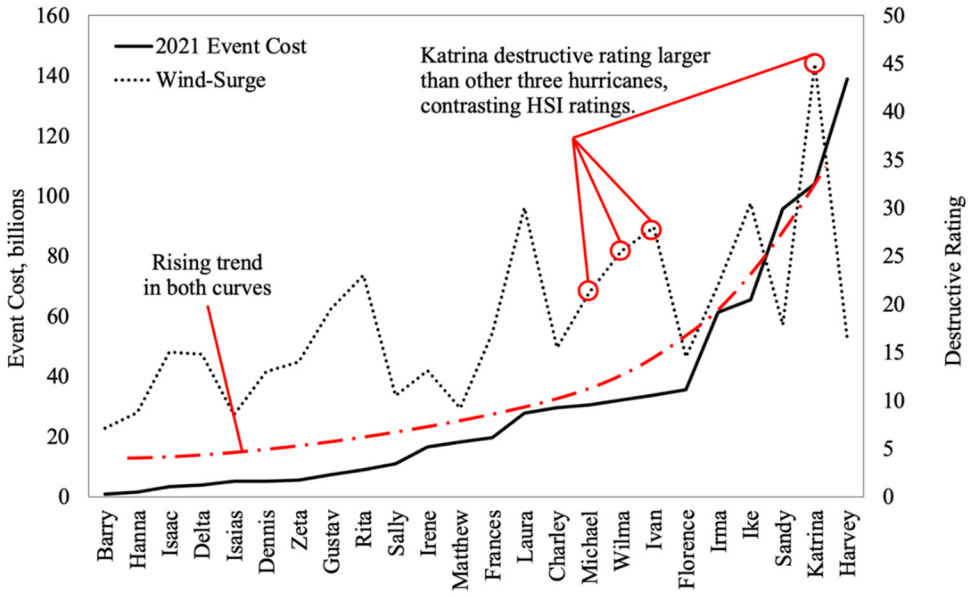

Figure 10. WSI vs. 2021 event cost.

A few hurricanes did not have ratings that followed the cost trend. Hurricane Harvey was rated far below Katrina, though Harvey is the costliest hurricane to date. Other phenomena that can contribute to damage include tornadoes, rainfall, and rip currents. Harvey caused record-breaking flooding with over 4.25ft of flooding in the Copano Bay area of Houston, Texas. Some Copano Bay areas received over 3.25ft of flooding in 40 hours [25]. Flooding was the main contributing factor to the high cost of Harvey. Geographical location contributes to the cost as well. The maximum wind speeds and surge height of Ike and Laura were 110mph and 150mph, 20ft, and 18ft respectively. Though wind and surge were similar, Ike cost $65.5 billion versus Laura's $27.72 billion. Hurricane Laura made landfall in Lousianna a less populated area. There were not many cities near Cameron; the coastal land is mostly a national wildlife refuge. Hurricane Ike made landfall in Galveston, TX, a more densely populated area than Cameron, LA. Comparing the surge and wind speed of hurricanes Ike and Laura, it is likely Hurricane Laura had a smaller impact due to the location and population density. For a list of SS, HSI, and Wind-Surge ratings,

refer to Table 6. In Table 6, every historical hurricane used in this study with its corresponding total cost in billions is listed. The cost of each hurricane is related to an estimate of all infrastructure damage caused by the hurricane. Each corresponding Saffir-Simpson, HSI, and Wind-Surge rating is also listed. The Saffir-Simpson rating is based on the one-minute maximum sustained wind speed when the hurricane hit land. The HSI values were gathered directly from [15]. The Wind-Surge rating was created from this study and uses the wind rating provided by HSI along with the maximum surge height for each hurricane.

Table 6. Destructive rating for historic hurricane events.

Event	2021 Event Cost (Billions)	Saffir-Simpson	HSI	Wind-Surge
Barry	0.86	1	8	7
Hanna	1.50	1	11	9
Isaac	3.43	1	14	15
Delta	3.93	4	17	15
Isaias	5.14	1	11	9
Dennis	5.15	4	18	13
Zeta	5.60	3	14	14
Gustav	7.32	1	20	20
Rita	8.92	5	28	23
Sally	10.99	2	13	11
Irene	16.62	3	18	13
Matthew	18.29	5	9	9
Frances	19.63	4	26	17
Laura	27.72	4	30	30
Charley	29.60	4	23	16
Michael	30.55	5	33	21
Wilma	32.12	4	33	26
Ivan	33.83	5	32	28
Florence	35.55	4	13	15
Irma	61.31	5	32	22
Ike	65.50	2	27	31
Sandy	95.66	2	14	18
Katrina	104.03	4	36	45
Harvey	138.83	3	22	16

Table 7 provides all one-minute maximum sustained wind speed and maximum surge height values for each historical hurricane event. The location of each event is also listed. These are the towns used in determining the county population factor.

Table 7. Data index for historic hurricanes.

Event	Year	Landfall Locations	Surge, ft	Max Wind Speed, mph
Barry	2019	Marsh Island, LA	6.1	75
Hanna	2020	Padre Island, TX	6.2	90
Delta	2020	Creole, LA	9.3	140
Zeta	2020	Cocodrie, LA	10.0	115
Isaac	2012	Plaquemines Parish	11.0	80
Dennis	2005	Pensacola, FL	7.0	150
Isaias	2020	Ocean Isle Beach, NC	6.0	85
Gustav	2008	Cocodrie, LA	12.5	55
Rita	2005	Cameron Parish, LA	12.0	175
Sally	2020	Cutler Bay, FL	7.0	110
Matthew	2016	McClellanville, SC	7.7	165
Irene	2011	Cape Lookout, NC	7.1	121
Frances	2004	Hutchinson Island, FL	7.0	145
Laura	2020	Cameron, LA	18.0	150
Michael	2018	Tyndall Air Force Base, FL	7.7	160
Charley	2004	Cayo Costa, FL	7.0	150
Florence	2018	Wrightsville Beach, NC	11.0	150
Ivan	2004	Gulf Shores, AL	15.0	165
Wilma	2005	Marco Island, FL	12.0	150
Ike	2008	Galveston, TX	20.0	110
Irma	2017	Cudjoe Key, FL	9.0	177
Sandy	2012	Atlantic City, NJ	13.9	110
Katrina	2005	New Orleans, LA	30.0	140
Harvey	2017	Rockport, TX	8.4	133

4b. Analysis Verification through Scaled Fluid-Structure Experimentation

A controlled scaled wave experiment was performed to provide validation for analytical modeling for more complex fluid-structure interaction demands. When a fluid-structure interaction is scaled down, there are fluid scaling effects that cause the results to be inaccurate. One option to compensate for those effects in waves is Froude similitude. Froude similitude is appropriate for gravity and inertial force dominate phenomena and is the most commonly used similitude in fluid dynamics [26]. It is used for highly turbulent phenomena where friction effects are negligible. The scaling factor, λ, is the ratio of a characteristic length of the full-size model to the corresponding length in the reduced-size model (see Table 8). Due to limited instrumentation and resources, a comparison of the response of the structure validated the analytical models.

Table 8. Froude scaling factors.

Parameter	Scaling Factor
Length	λ
Time	$\sqrt{\lambda}$
Pressure	λ
Stress	λ
Force	λ^2

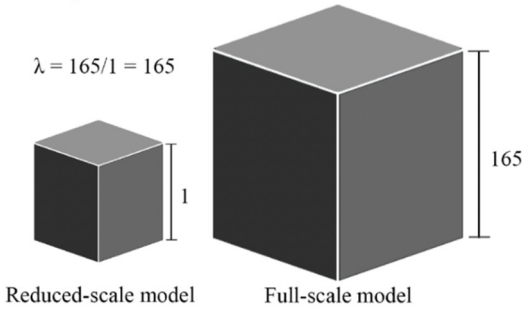

There can also be scaling effect issues with wind; the most prominent effects are due to the Reynolds number. The Reynolds number must be kept the same from large to small scale, but no wind was used for the experimental model. Instead, the analytical simulation used pressure to represent the wind to eliminate the Reynolds number scaling error.

The wind-surge wave chamber, crane, and dock were rectangular prisms. To create a wave, one end of the box was lifted and dropped. A pressure gauge was attached to the front of the crane, and the water pressure resulting from the wave was recorded. Figure 11 shows the wave progression during the validation experiment and Figure 12 shows the instrumentation included on the Crane 1 scale model for measuring fluid contact pressure.

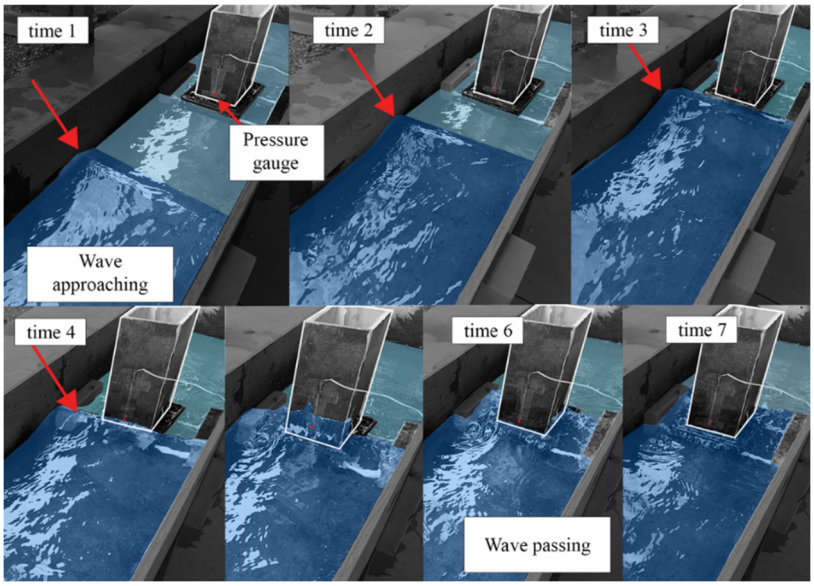

Figure 11. Progression of wave during experiment.

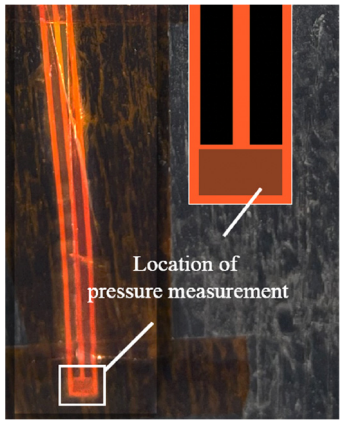

Figure 12. Pressure gauge considered in validation experiment.

The experimental crane and Crane 1 showed behavior responses that were similar in shape. There was a sudden increase in pressure when the wave initially hit, and a second pulse of pressure while the wave was in contact as seen in Figure 13. Data was obtained from one element on the simulated crane that had the same location and size properties of the pressure gauge used in the experiment.

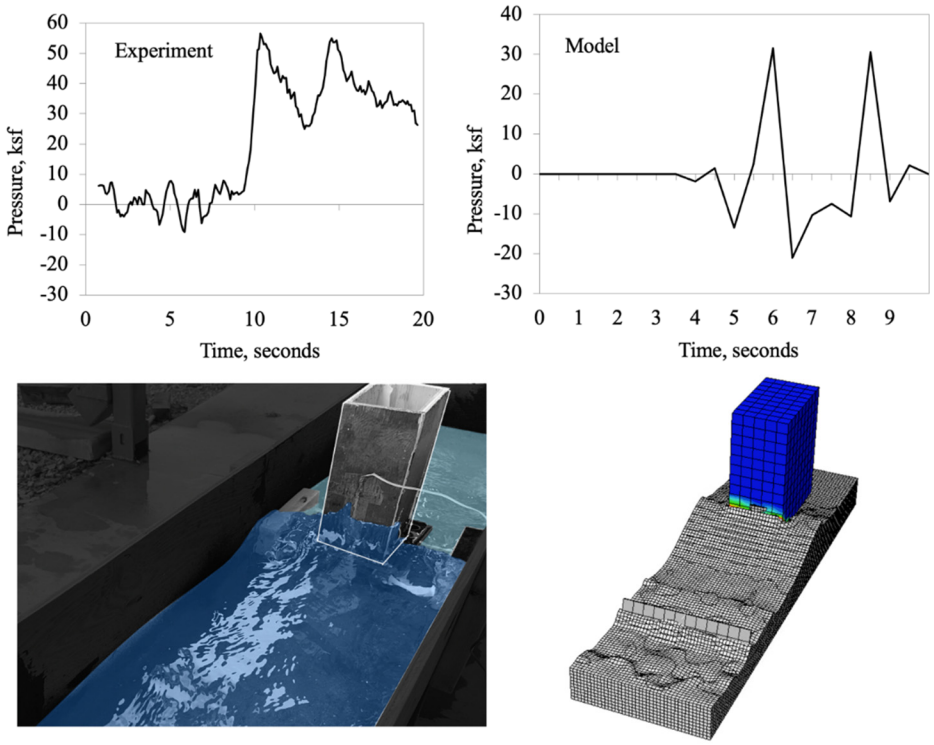

Figure 13. Experimental crane vs. Crane 1

4c. Observations from Historical Damage Review and Fluid-Structure Interaction Simulations

The SS, HSI, and Wind-Surge destructive rating systems were compared using historical hurricane damage data. The SS scale was not accurate in determining the damage resulting from a hurricane. Only maximum wind speed was considered in SS though there are many other contributing factors. Hurricane Delta cost 15% more than Isaac, but Delta was rated to be 300% more destructive. There was little consistency in a lower destructive rating and a lower event cost using SS. HSI showed some improvement over SS by including wind field in the ratings. The larger 50-point scale provided the opportunity for better distinction between hurricane characteristics and the potential damage caused by each characteristic. There were still large jumps between destructive ratings of hurricanes that were similar in event cost. The Wind-Surge showed improvement over HSI by including storm surge in the ratings. Some hurricanes that had comparable ratings in HSI were distinguished in Wind-Surge. Other hurricane ratings, such as Harvey, received a lower rating in Wind-Surge than HSI though it should have received a higher rating. However, the data did improve in accuracy when surge was included.

The interaction simulations were compared using the maximum average stress of the entire crane, S. Simulations with no wave applied, only wind, had S values of 1 to 2ksf. When a wave was applied, S values ranged from 100-400ksf. The wind had become negligible when a wave was applied.

The shape of the S curve changed when a surge was introduced; there were 3 pulses instead of one as seen in Figure 14. The only force on the structure when no surge was present was the wind until the wave hit. When there was surge present, the water was constantly in contact with the structure. The first two pulses are due to the pull of the water as the applicator displaced to create the wave. The third pulse is the impact of the wave.

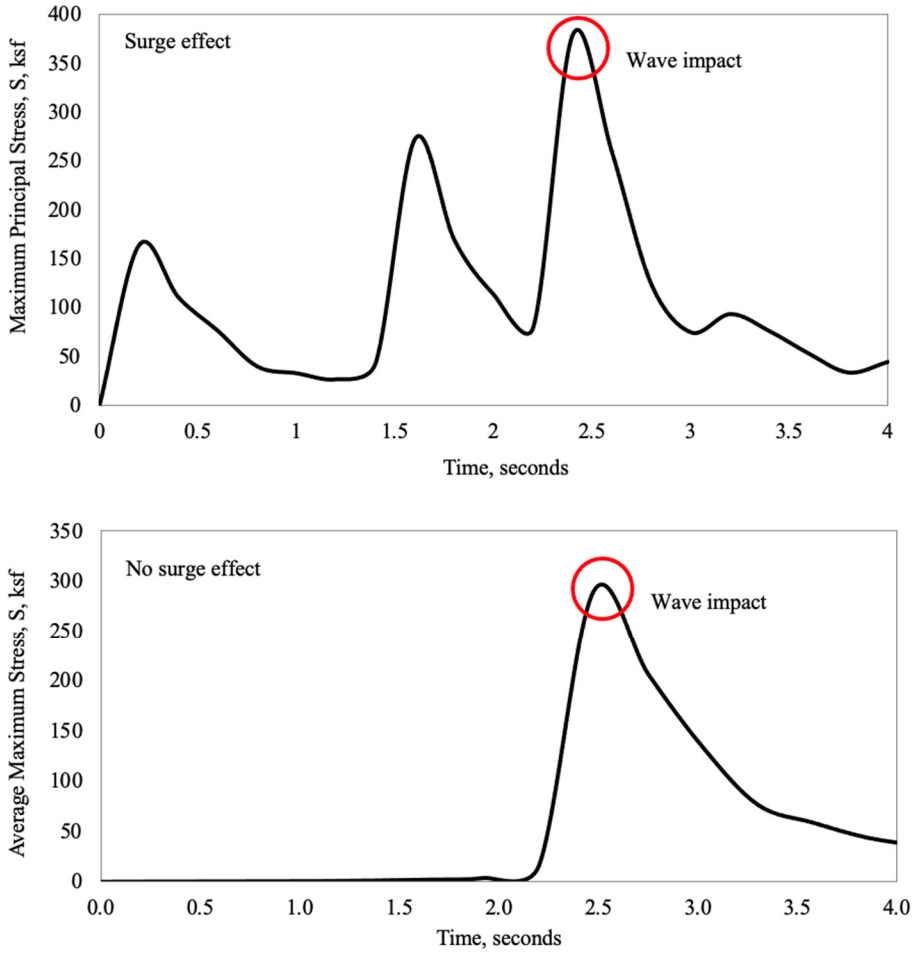

Figure 14. Typical shape of S with no surge effect.

4d. Effect of Wind and Wave Demands Without Surge

Figure 15 shows S, the maximum stress, increases as wave height increases on average. The 10ft wave was not large enough to enforce more load on the crane than the wind provided. The 14ft wave caused an increase in S for all wind speeds. However, the fastest wind speed did not always correlate to the largest S value. There was inconsistency for wave heights 14 and 18ft. 100mph/14ft simulation produced a larger maximum principal stress than 120mph/14ft. This happened again with the 60mph/18ft simulation being the largest of all 18ft wind speeds. The inconsistency in faster winds creating larger stresses began when the waves were large enough to impact the stress. The stress that results from waves is semi-unpredictable. It would be expected

for the 120mph wind to always cause the most stress, but that did not happen for 2 of 5 wave heights. There was a constant increase in S for wind speeds of 120, 100, and 80 mph as wave height increased. 60 and 0mph had outliers resulting in no trend.

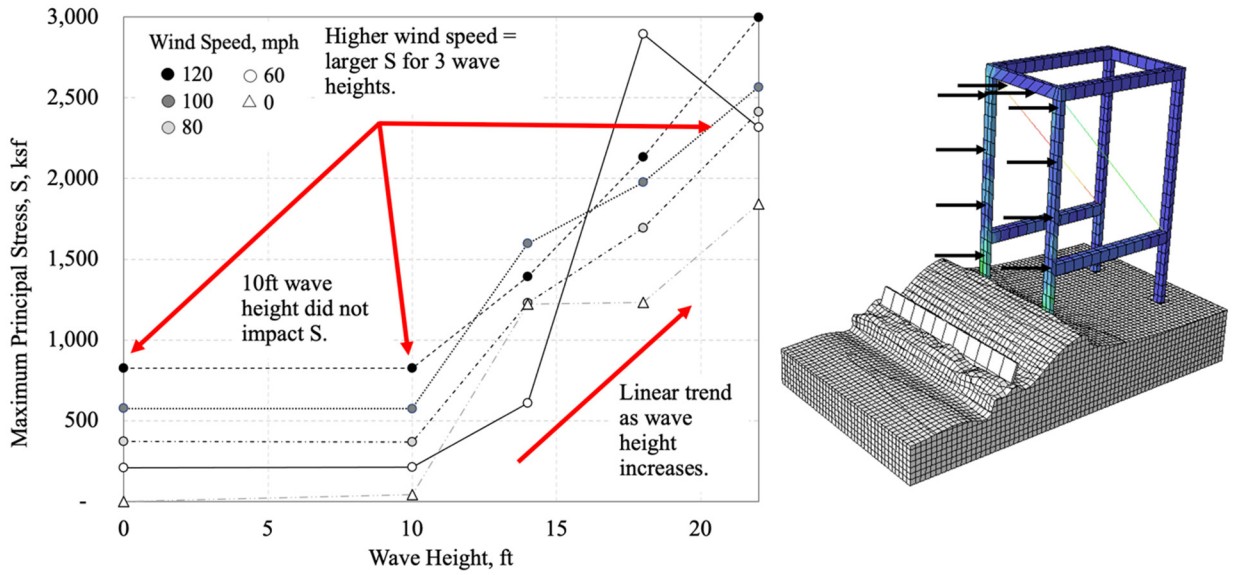

Figure 15. Maximum principal stress of wind and wave demands without surge.

4e. Effect of Surge on Wind and Wave Demands

Like simulations with no surge, the stresses increased with each wave height increase. However, the change in S increased each time as well. Figure 16 shows a trend related to an exponential curve unlike the linear trend in Figure 15. There was no consistency in a higher wind speed resulting in a larger stress. The 120mph simulations did not have the largest S in any instance where a wave was present. The surge allowed for more water to structure contact during the length of the simulation, giving the water more influence in the loading. The structure was only in contact with water during wave contact when there was no surge. At least 10ft of water was constantly pushing and pulling on the structure. The shapes of the S curves in Figure 14 show the interaction with water before wave impact.

Between 18 and 24ft there was a large increase in S. This could have been due to the wave being a breaking wave, though the simulations without surge did not have a significant difference between non-breaking and breaking waves. Figure 17 explains the difference between a breaking and non-breaking wave. Table 9 provides each simulation, wind speed, and wave height combination used with the corresponding maximum average stress value recorded.

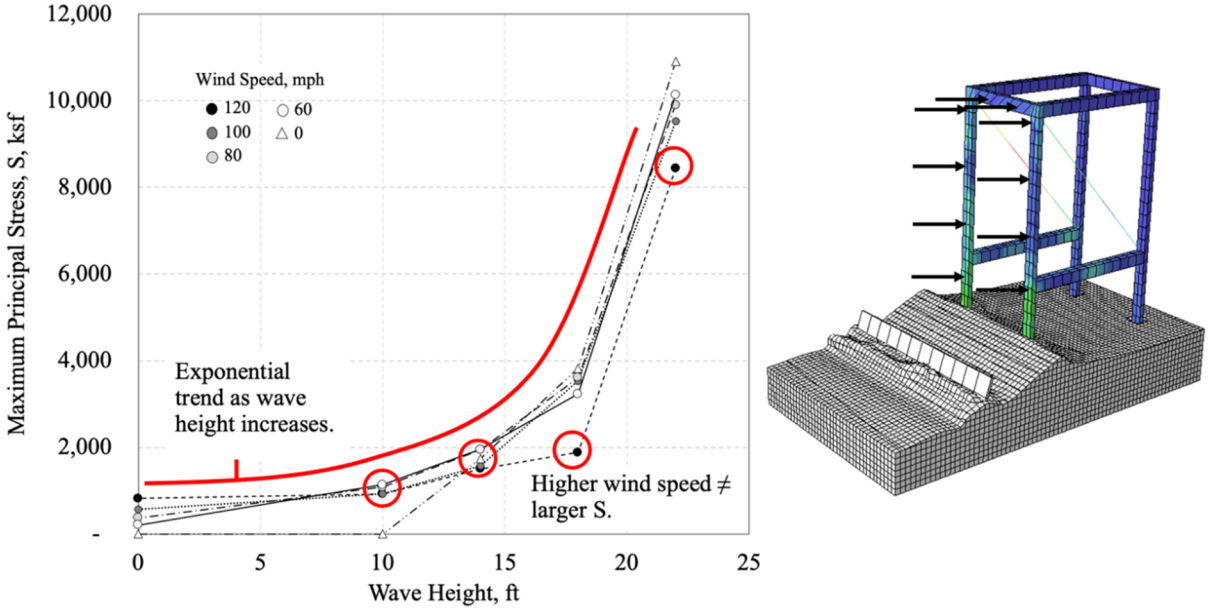

Figure 16. Simulation results grouped by wave height, 10ft surge.

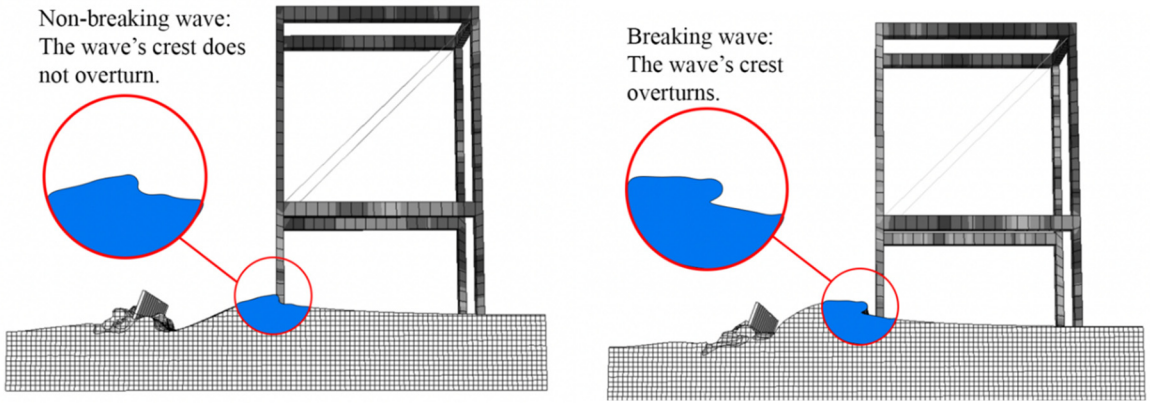

Figure 17. Non-breaking versus breaking wave.

Table 9. Load combination and results for each simulation with 10ft surge.

Simulation #	Wind, mph	Wave Height, ft	Maximum Average Stress, ksf
25	120	40	342
26		30	209
27		24	118
28		20	98
29	100	40	395
30		30	308
31		24	139
32		20	96
33	80	40	338
34		30	316
35		24	132
36		20	95
37	60	40	393
38		30	319
39		24	134
40		20	95
41	0	40	379
42		30	336
43		24	135
44		20	106

5. Conclusions

Tropical storm destruction is dependent on numerous variables including storm surge, wind speed, rainfall, wave height, etc. The analytical models in this study focused on the coupled effects of wind speed, wave height, and storm surge. The storm severity prediction tool did not consider wave height; it considered wind and storm surge; however, because monetary values were used to compare the resulting damage from historic hurricanes, all variables were included in the monetary data. This did not allow for a direct comparison of costs attributed to storm surge versus wind speed. The storm severity prediction tool suggested there is a need to rate tropical storms using more than only maximum sustained wind speed. Storm surge coupled with wind speed can provide a more accurate representation of the potential total damage of a hurricane.

Analyses suggest that when surge conditions are considered, wave height and wave type dominate the structural demand over increases in wind speed. For loading scenarios impacted by surge, there was little-to-no increase in stress on the structure when only wind speed increased. The developed wind-surge damage index and analytical model findings suggest that both storm surge and wave loading should be considered in port infrastructure design to reduce damage costs and improve resiliency.

References

1. ITA (2018). Maritime Services Trade Data, *International Trade Administration,* https://www.trade.gov/maritime-services-trade-data, accessed 2/11//2022.

2. Haveman, J.D. and H.J. Shatz (2006). Protecting the nation's seaports: Balancing security and cost. *Public Policy Institute of California.*

3. AAPA (2005). Hurricane-Affected U.S. Gulf Coast Ports Coming Back Strong, *American Association of Port Authorities,* https://www.aapa-ports.org/advocating/PRdetail.aspx?itemnumber=1452, accessed 2/3/2022

4. Mosbrucker, K (2020). Louisiana ports hit by Hurricane Laura battered as ship traffic restricted; industry prepares return, *The Advocate*, https://www.theadvocate.com/baton_rouge/news/business/article_74d5055c-eec4-11ea-ad85-53af04a4d061.html, accessed 12/7/2020

5. US Inflation Calculator (2022). Consumer Price Index Data from 1913 to 2022, https://www.usinflationcalculator.com/inflation/consumer-price-index-and-annual-percent-changes-from-1913-to-2008/, accessed 11/3/2021

6. Powell, M.D. and T.A. Reinhold (2007). Tropical Cyclone Destructive Potential by Integrated Kinetic Energy, *American Meteorological Society. p. 513-526.*

7. Lombardo, F., et al. (2017). Observations of building performance under combined wind and surge loading from hurricane Harvey, *American Geophysical Union, Fall Meeting.*

8. McCarthy, P., E. Soderberg, and A. Dix (2009). Wind Damage to Dockside Cranes: Recent Failures and Recommendations, *ASCE: TCLEE 2009. p. 516-527.*

9. Chock, G., et al. (2013). Tohoku, Japan, Earthquake and Tsunami of 2011: Performance of Structures under Tsunami Loads, *ASCE.*

10. NHC (2021). The Saffir-Simpson Hurricane Wind Scale, *National Hurricane Center*, https://www.nhc.noaa.gov/pdf/sshws.pdf, accessed 3/4/2022

11. D., K.R., J.R. Rhome, and D.P. Brown (2005). Tropical Cyclone Report Hurricane Katrina, *National Hurricane Center*, https://www.nhc.noaa.gov/data/tcr/AL122005_Katrina.pdf, accessed 12/3/2021

12. Beven II, J.L., R. Berg, and A. Hagen (2019). National Hurricane Center Tropical Cyclone Report Hurricane Michael, *National Hurricane Center,* https://www.nhc.noaa.gov/data/tcr/AL142018_Michael.pdf, accessed 12/3/2021

13. NHC (2021). Introduction to Storm Surge, *National Hurricane Center*, https://www.nhc.noaa.gov/surge/, accessed 2/2/2022

14. Berg, R. (2009). Tropical Cyclone Report Hurricane Ike, *National Hurricane Center*, https://www.nhc.noaa.gov/data/tcr/AL092008_Ike.pdf, accessed 2/2/2022

15. Hebert, C.G., R.A. Weinzapfel, and M.A. Chambers (2019). Hurricane Severity Index: A New Way of Estimating Hurricane Destructive Potential. *StormGeo*.

16. The Disaster Center (1999). TPC NHC -- Saffir -- Simpson Hurricane Scale. *The Disaster Center*, https://www.disastercenter.com/hurrican/scale.htm, accessed 3/2/2022

17. Pielke, R.A. and C.W. Landsea (1998), Normalized Hurricane Damages in the United States: 1925–95*. Weather and Forecasting, 13(3): p. 621-631.*

18. Pielke Jr., R., et al. (2008). *Normalized Hurricane Damage in the United States: 1900-2005*. ASCE: Natural Hazards Review.

19. Pielke, R.A., et al. (2008). *Normalized Hurricane Damage in the United States: 1900–2005.* Natural Hazards Review 9(1): p. 29-42.

20. USCB (2022). Evaluation Estimates, *United States Census Bureau*, https://www.census.gov/programs-surveys/popest/technical-documentation/research/evaluation-estimates.html, accessed 2/10/2022

21. U.S. Bureau of Economic Analysis (2022), Gross Domestic Product: Implicit Price Deflator [GDPDEF], retrieved from FRED, *Federal Reserve Bank of St. Louis*; https://fred.stlouisfed.org/series/GDPDEF, 2/3/2022.

22. U.S. Bureau of Economic Analysis (2022), Current-Cost Net Stock of Fixed Assets and Consumer Durable Goods [K1WTOTL1ES000], retrieved from FRED, *Federal Reserve Bank of St. Louis*; https://fred.stlouisfed.org/series/K1WTOTL1ES000, 2/3/2022.

23. Dassalt Systèmes (2014), *Abaqus/CAE User's Guide (6.14),* http://130.149.89.49:2080/v6.14/pdf_books/CAE.pdf, accessed 12/10/2021.

24. Eulerian analysis (2017). https://abaqus-docs.mit.edu/2017/English/SIMACAEANLRefMap/simaanl-c-eulerianananalysis.htm, accessed 12/10/2021

25. National Weather Service Corpus Christi, TX Weather Forecast Office (2017). Category 4 Hurricane Harvey: South Texas Landfall & Impacts from August 25th to 29th, 2017. *National Weather Service,* https://www.weather.gov/crp/hurricane_harvey, accessed 12/3/2021

26. Heller, V. (2021). Model-Prototype Similarity, http://www.drvalentinheller.com/Dr%20Valentin%20Heller_files/Heller_Model-Prototype%20Similarity.pdf, accessed 2/16/2022

27. Cangialosi, J.P., A.B. Hagen, and R. Berg (2019). National Hurricane Center Tropical Cyclone Report Hurricane Barry, *National Hurricane Center*, https://www.nhc.noaa.gov/data/tcr/AL022019_Barry.pdf , accessed 12/3/2021

28. Brown, D.P., R. Berg, and B. Reinhart (2021). National Hurricane Center Tropical Cyclone Report Hurricane Hanna, *National Hurricane Center,* https://www.nhc.noaa.gov/data/tcr/AL082020_Hanna.pdf, accessed 12/3/2021

29. Cangialosi, J.P. and R. Berg (2021). National Hurricane Center Tropical Cyclone Report Hurricane Delta, *National Hurricane Center*, https://www.nhc.noaa.gov/data/tcr/AL262020_Delta.pdf, accessed 12/3/2021

30. Blake, E., R. Berg, and A. Hagen (2021), National Hurricane Center Tropical Cyclone Report Hurricane Zeta, *National Hurricane Center*, https://www.nhc.noaa.gov/data/tcr/AL282020_Zeta.pdf, accessed 12/3/2021

31. Mainelli, M. (2006). Tropical Cyclone Report Hurricane Isaac. *National Hurricane Center*, https://www.nhc.noaa.gov/data/tcr/AL102006_Isaac.pdf, accessed 12/3/2021

32. The City Wire Staff (2012). Hurricane Isaac may cost insurers $2 billion, *Talk Business and Politics*, https://talkbusiness.net/2012/08/hurricane-isaac-may-cost-insurers-2-billion/, accessed 4/19/2022

33. Beven, J. (2005). Tropical Cyclone Report Hurricane Dennis, *National Hurricane Center,* https://www.nhc.noaa.gov/data/tcr/AL042005_Dennis.pdf, accessed 12/3/2021

34. Latto, A., A. Hagen, and R. Berg (2021). National Hurricane Center Tropical Cyclone Report Hurricane Isaias, *National Hurricane Center*, https://www.nhc.noaa.gov/data/tcr/AL092020_Isaias.pdf, accessed 12/3/2021

35. Beven III, J.L. and T.B. Kimberlain (2008). Tropical Cyclone Report Hurricane Gustav, *National Hurricane Center*, https://www.nhc.noaa.gov/data/tcr/AL072008_Gustav.pdf, accessed 12/3/2021

36. Knabb, R.D., D.P. Brown, and J.R. Rhome (2005). Tropical Cyclone Report Hurricane Rita, *National Hurricane Center*, https://www.nhc.noaa.gov/data/tcr/AL182005_Rita.pdf, accessed 12/3/2021

37. Berg, R. and B.J. Reinhart (2021). National Hurricane Center Tropical Cyclone Report Hurricane Sally, *National Hurricane Center*, https://www.nhc.noaa.gov/data/tcr/AL192020_Sally.pdf, accessed 12/3/2021

38. Stewart, S.R. (2007). National Hurricane Center Tropical Cyclone Report Hurricane Matthew, *National Hurricane Center*, https://www.nhc.noaa.gov/data/tcr/AL142016_Matthew.pdf, accessed 12/3/2021

39. Avila, L.A. and J. Cangialosi (2011). Tropical Cyclone Report Hurricane Irene, *National Hurricane Center*, https://www.nhc.noaa.gov/data/tcr/AL092011_Irene.pdf, accessed 12/3/2021

40. Beven II, J.L. (2004). Tropical Cyclone Report Hurricane Frances, *National Hurricane Center*, https://www.nhc.noaa.gov/data/tcr/AL062004_Frances.pdf, accessed 12/3/2021

41. Pasch, R.J., et al. (2021). National Hurricane Center Tropical Cyclone Report Hurricane Laura, *National Hurricane Center*, https://www.nhc.noaa.gov/data/tcr/AL132020_Laura.pdf, accessed 12/3/21

42. Pasch, R.J., D.P. Brown, and E.S. Blake (2004). Tropical Cyclone Report Hurricane Charley, *National Hurricane Center,* https://www.nhc.noaa.gov/data/tcr/AL032004_Charley.pdf, accessed 12/3/21

43. Stewart, S.R. and R. Berg (2019). National Hurricane Center Tropical Cyclone Report Hurricane Florence, *National Hurricane Center*, https://www.nhc.noaa.gov/data/tcr/AL062018_Florence.pdf, accessed 12/3/21

44. Stewart, S.R. (2004). Tropical Cyclone Report Hurricane Ivan, *National Hurricane Center*, https://www.nhc.noaa.gov/data/tcr/AL092004_Ivan.pdf, accessed 12/3/21

45. Pasch, R.J., et al. (2006). Tropical Cyclone Report Hurricane Wilma, *National Hurricane Center,* https://www.nhc.noaa.gov/data/tcr/AL252005_Wilma.pdf, accessed 12/3/21

46. Cangialosi, J.P., A.S. Latto, and R. Berg (2021). National Hurricane Center Tropical Cyclone Report Hurricane Irma, *National Hurricane Center*, https://www.nhc.noaa.gov/data/tcr/AL112017_Irma.pdf, accessed 12/3/21

47. Blake, E.S., et al. (2013), Tropical Cyclone Report Hurricane Sandy, *National Hurricane Center*, https://www.nhc.noaa.gov/data/tcr/AL182012_Sandy.pdf, accessed 12/3/21

48. Blake, E.S. and D.A. Zelinsky (2018). National Hurricane Center Tropical Cyclone Report Hurricane Harvey, *National Hurricane Center*, https://www.nhc.noaa.gov/data/tcr/AL092017_Harvey.pdf, accessed 12/3/21